

Signal versus Background Interference in $H^+ \rightarrow t\bar{b}$ Signals for MSSM Benchmark Scenarios

Abdesslam Arhrib^a, Duarte Azevedo^b, Rachid Benbrik^c, Hicham Harouiz^c, Stefano Moretti^d,
Riley Patrick^e, Rui Santos^{b,f}

^aFaculty of Sciences and Techniques, Abdelmalek Essaadi University, B.P. 416, Tanger, Morocco

^bCentro de Física Teórica e Computacional, Faculdade de Ciências, Universidade de Lisboa, Campo Grande, Edifício C8, 1749-016 Lisboa, Portugal

^cMSISM Team, Faculté Polydisciplinaire de Safi, Sidi Bouzid, B.P. 4162, Safi, Morocco

^dSchool of Physics and Astronomy, University of Southampton, Southampton, SO17 1BJ, United Kingdom

^eARC Center of Excellence for Particle Physics at the Terascale, Department of Physics, University of Adelaide, 5005 Adelaide, South Australia

^fISEL - Instituto Superior de Engenharia de Lisboa, Instituto Politécnico de Lisboa, 1959-007 Lisboa, Portugal

Abstract

In this paper, we investigate sizeable interference effects between a heavy charged Higgs boson signal produced dominantly via $gg \rightarrow t\bar{b}H^-$ (+ c.c.) followed by the decay $H^- \rightarrow b\bar{t}$ (+ c.c.) and the irreducible background given by $pp \rightarrow t\bar{t}b\bar{b}$ topologies at the Large Hadron Collider (LHC). We show that it may be possible that such effects could spoil current H^\pm searches where signal and background are normally treated separately. The reason for this is that a heavy charged Higgs boson can have a large total width, in turn enabling such interferences, altogether leading to potentially very significant alterations, both at the inclusive and exclusive level, of the yield induced by the signal alone. This therefore implies that currently established LHC searches for such wide charged Higgs bosons might require modifications. We show such effects quantitatively using two different benchmark configurations of the minimal realisation of Supersymmetry, wherein such H^\pm states naturally exist. However, on the basis of the limited computing resources available, we are unable to *always* bring the statistical error down to a level where all such interference effects are unequivocal, so that we advocate dedicated experimental analyses to confirm this with higher statistics data samples.

1 Introduction

After the discovery of a Higgs-like particle at Large Hadron Colliders (LHC) a few years ago [1,2], a significant amount of both theoretical and experimental activities have taken place trying to identify the nature of this object. The mass of such a particle and its couplings to some Standard Model (SM) particles are now measured with a good precision [3,4]. Their values indicate that such a Higgs-like particle is light and its properties (spin, CP quantum numbers and interactions) are consistent with those of the SM Higgs boson.

However, there are many theoretical and experimental indications that show that the SM can only be an effective theory of a more fundamental one that still needs to be discovered. Many Beyond the SM (BSM) scenarios have been put forward over the years and it is fair to say that one stems as the most appealing one - Supersymmetry (SUSY). This is because it solves the well-known hierarchy problem of the SM by protecting the Higgs mass from unstable higher order corrections thanks to the new symmetry between fermions and bosons that it predicts [5]. Furthermore, SUSY also has the capability to address the Dark Matter (DM) and gauge unification problems of the SM, indeed, without any proliferation of fundamental parameters if one assumes that SUSY can in turn be viewed as an effective realisation of some Grand Unified Theory (GUT), like Supergravity [6,7]. The Minimal Supersymmetric Standard Model (MSSM) is the simplest realisation of SUSY that predicts a light Higgs boson h^0 that can be identified as the observed 125 GeV Higgs-like particle and can be as successful as the SM when confronted with experimental data, yet it can surpass it in all the above respects.

The Superpotential of the MSSM has to be holomorphic, thus one needs to introduce at least two Higgs doublets fields, one more than in the SM. One of these generates masses for up quarks and the other one generate masses for down quarks and charged leptons. From the 8 degrees of freedom present in such a 2-Higgs Doublet Model (2HDM), 3 are acquired by the longitudinal components of the gauge bosons W^\pm and Z^0 , so that the latter get a mass too, and the remaining 5 appears as new Higgs particles: 2 CP-even h and H (with $M_{h^0} < M_{H^0}$), one CP-odd A and a pair of charged ones H^\pm . Discovery of any such new states would be unmistakable evidence of BSM physics, yet, only charged Higgs states would be a clear hint towards a 2HDM structure, as required by the MSSM, as additional neutral Higgs states could be attributed to singlet structures entering an extended Higgs sector.

At a hadron collider, production of charged Higgs bosons proceeds through many channels. If the charged Higgs boson is light (i.e., $M_{H^\pm} < m_t + m_b$), it can be produced from top or anti-top decay: i.e., $gg, q\bar{q} \rightarrow t\bar{t}$ followed by, e.g., $\bar{t} \rightarrow bH^-$ (+ c.c.). Given the fact that the $t\bar{t}$ cross section is very large, this mechanism would give an important source of light charged Higgs states. After the top-bottom threshold (i.e., $M_{H^\pm} > m_t + m_b$), a charged Higgs boson can be produced in association with top-bottom pairs, i.e., $bg \rightarrow tH^-$ [8]. In fact, these two channels are captured at once by the $gg \rightarrow t\bar{b}H^-$ (+ c.c.) ‘complete’ process, as explained in [9,10]. There exist other production mechanisms too, such as $pp \rightarrow H^+H^-$, $pp \rightarrow A^0H^\pm$, $pp \rightarrow H^\pm W^\mp$, etc. which are however subleading compared to the previous ones¹.

At the LHC, a light charged Higgs boson, with $M_{H^\pm} < m_t + m_b$, can be detected from $t\bar{t}$ production followed by top or anti-top quark decay $t \rightarrow bH^+$ if the H^- state decays dominantly to $\tau\nu$. ATLAS and CMS have already set a limit on $\text{BR}(t \rightarrow bH^+) \times \text{BR}(H^+ \rightarrow \tau\nu)$ [12–15], which can be translated into a limit on the $(M_{H^\pm}, \tan\beta)$ plane, where $\tan\beta$ is the ratio of the two Higgs doublet vacuum expectation values (VEVs). In the MSSM, for some specific benchmark scenarios, charged Higgs bosons with mass less than about 160 GeV are ruled out for almost any value of $\tan\beta$ [14,15]. However, heavy charged Higgs states, with $M_{H^\pm} > m_t + m_b$, are generally allowed as they would decay dominantly into $t\bar{b}$, which is a rather difficult final state to extract due to large reducible and irreducible backgrounds associated with jets emerging from $H^- \rightarrow t\bar{b}$ decays. Even then, one could still get a moderate signal from such a channel for small $\tan\beta \leq 1.5$ or large $\tan\beta \geq 40$ [16,17]. Another possibility for detecting heavy charged Higgs states would be the search for $H^+ \rightarrow \bar{\tau}\nu_\tau$ (i.e., like the preferred one for a light state), which enjoys a smaller background in comparison. At the LHC Run 2, both channels have been searched for and no excess over the background

¹For a recent review, see [11].

only hypothesis have been reported. Therefore, limits are set on $\sigma(pp \rightarrow tH^-) \times \text{BR}(H^- \rightarrow \bar{t}b/\tau\bar{\nu}_\tau)$ (+ c.c.) [18–21]. In the MSSM, one can have additional SUSY channels that can contribute to H^\pm production and/or decay, e.g., production from squark/gluino cascades [22, 23] and/or decays into chargino-neutralino states [24, 25], though these require special MSSM configuration assumptions, hence they are not currently pursued by ATLAS and CMS.

The current highest priority, in relation to charged Higgs boson searches at the LHC, is to further establish the $H^+ \rightarrow t\bar{b}$ decay channel in the heavy mass region. With this in mind, using the framework of a generic 2HDM [26], we have investigated the possibility of having large interference effects between signals from a heavy charged Higgs boson via $bg \rightarrow tH^- \rightarrow tW^-A \rightarrow tW^-b\bar{b}$ (and similarly for h and H) and the irreducible background from $bg \rightarrow tW^-b\bar{b}$ processes. Therein, it was shown that such interference effects can modify any dedicated charged Higgs boson searches where signal and background are treated separately, which is the case for all aforementioned experimental analyses.

The purpose of this paper is to address similar issues for the MSSM, i.e., to quantify the impact of interference effects between the ‘complete’ signal $pp \rightarrow t\bar{b}H^-$ and the irreducible background in the $H^- \rightarrow b\bar{t}$ decay channel. We will show that such effects are indeed large for heavy H^\pm masses for two MSSM benchmark scenarios, both for inclusive cross section calculations and after a full detector analysis. The plan of the paper is as follows. In the forthcoming section we describe the MSSM configurations used. Sect. 3 dwells on the MSSM spectra conducive to generate such large interference phenomena. Sect. 4 presents our numerical results. Finally, we conclude in Sect. 5.

2 Definition of the benchmark scenarios

At tree level, the MSSM Higgs sector is completely fixed by 2 parameters: $\tan\beta$ and a Higgs boson mass, e.g., the CP-odd one (M_{A^0}). One of the major predictions of SUSY is the presence of a light CP-even Higgs (lighter than Z boson at the lowest order) in the spectrum. However, high order corrections can shift such a mass in order to fit the observed Higgs-like particle mass [27–29]. It has been shown in [30] that high order corrections could raise the tree-level MSSM prediction for such a mass up to 135 GeV for large soft trilinear breaking terms and also that the theoretical uncertainties due to the unknown high order effects should be of the order of 3 GeV.

In the MSSM, the most important parameters relevant for the prediction of the masses, couplings and, hence, production cross sections and decay probabilities of the Higgs bosons are: $\tan\beta$, M_{A^0} , the soft SUSY-breaking masses for the stop and sbottom squarks (which, for simplicity, we assume all equal to a common mass parameter M_S), the soft SUSY-breaking gluino mass $m_{\tilde{g}}$, the Superpotential Higgs-mass parameter μ and the left-right mixing terms in the stop and sbottom mass matrices, i.e.,

$$X_t = A_t - \mu \cot\beta, \quad X_b = A_b - \mu \tan\beta, \quad (1)$$

respectively.

We use the PROSPINO public code [31] to compute the charged Higgs boson production cross section $\sigma(pp \rightarrow t(\bar{b})H^- + \text{c.c.})$, which includes Next-to-Leading Order (NLO) corrections to the $bg \rightarrow tH^- + \text{c.c.}$ (2-to-2) process. We use the inclusive cross section computed this way to test the viability of our proposed MSSM scenarios against data.

However, we adopt the tree-level $pp \rightarrow t\bar{b}H^- + \text{c.c.}$ (2-to-3) process for Monte Carlo (MC) event generation, because it produces a better description of the signal at the differential level in the detector region than the former channel (i.e., the additional b -(anti)quark is explicit in the phase space rather than integrated into the proton content) and because the corresponding irreducible background is only known at LO. This clearly implies that the normalisation used for the MC analysis is different from that used in the inclusive parameter scans, however, we note that we are primarily concerned here with the relative behaviour of signal, irreducible background and relative interference, rather than the overall normalisation. (Note that, hereafter,

Experiment	Luminosity [fb ⁻¹]	Label	Channel
LEP	–	[39]	$e^+e^- \rightarrow H^+H^- \rightarrow qq'qq'$
LEP	–	[40] (DELPHI)	$e^+e^- \rightarrow H^+H^- \rightarrow qq'qq'$
LEP	–	[40] (DELPHI)	$e^+e^- \rightarrow H^+H^- \rightarrow \tau\nu\tau\nu$
D0	1.000	[41] (D0)	$t \rightarrow bH^+ \rightarrow bqq'$
CDF	2.200	[42] (CDF)	$t \rightarrow H^+b$
CDF	0.192	[43] (CDF)	$t \rightarrow bH^+ \rightarrow b\tau\nu$
CDF	0.335	[44] (CDF)	$t \rightarrow bH^+ \rightarrow b\tau\nu$
D0	1.000	[41] (D0)	$t \rightarrow bH^+ \rightarrow b\tau\nu$
ATLAS, 7 TeV	0.035	ATLAS-CONF-2011-094	$t \rightarrow H^+b \rightarrow c\bar{s}b$
ATLAS, 7 TeV	4.600	[45]	$t \rightarrow H^+b$
ATLAS, 8 TeV	19.500	ATLAS-CONF-2014-050	$t \rightarrow bH^+ \rightarrow b\tau\nu$
ATLAS, 13 TeV	36.100	[15]	$pp \rightarrow tbH^+ \rightarrow tb\tau\nu$
ATLAS, 13 TeV	36.100	[15]	$t \rightarrow bH^+ \rightarrow b\tau\nu$
CMS, 8 TeV	19.700	CMS-PAS-HIG-14-020	$t \rightarrow bH^+ \rightarrow b\tau\nu$
CMS, 8 TeV	19.700	CMS-PAS-HIG-13-035	$t \rightarrow H^+b \rightarrow c\bar{s}b$
CMS, 8 TeV	19.700	CMS-PAS-HIG-16-030	$t \rightarrow H^+b \rightarrow c\bar{b}b$
CMS, 13 TeV	12.900	[19]	$t \rightarrow bH^+ \rightarrow b\tau\nu$
CMS, 13 TeV	35.900	CMS-PAS-HIG-18-014	$t \rightarrow H^+b \rightarrow c\bar{b}b$
ATLAS, 13 TeV	14.700	ATLAS-CONF-2016-088	$pp \rightarrow tbH^+ \rightarrow tb\tau\nu$
ATLAS, 13 TeV	36.100	[21]	$pp \rightarrow tbH^+ \rightarrow ttbb$

Table 1: Constraints on charged Higgs boson processes implemented in HiggsBounds and used in our analyses.

we always sum over both H^+ and H^- .) Both PROSPINO and FeynHiggs [32, 33] use the same (on-shell) renormalisation scheme, therefore, the input values of the MSSM parameters can be passed seamlessly from the Higgs spectrum generator to the cross section calculator. The MSSM parameter space is already highly constrained by asking that one of the CP-even neutral scalar states should mimic the properties of the SM-like Higgs boson observed at LHC while the additional Higgs bosons should satisfy the existing constraints obtained from ATLAS and CMS from different channels. For this purpose, the FeynHiggs code is linked to HiggsBounds-5.2.0beta [34–37] and HiggsSignals-2.2.0beta [38] allowing us to check the consistency of our parameter space against various LHC as well as Tevatron and LEP constraints. We list in Tab. 1 the specific charged Higgs boson searches that have been included in HiggsBounds. Additionally, a variety of lower energy constraints have been enforced, such as $B \rightarrow \tau\nu$, $B_{d,s} \rightarrow \mu^+\mu^-$, $B \rightarrow X_s\gamma$ and $\Delta m_{s,d}$ (see details in [46]).

All of the MSSM benchmark scenarios adopted in our analysis are characterised by relatively large values of the ratio X_t/M_S . This ensures that the mass of the SM-like Higgs state falls within the required range without the need for an extremely heavy stop. In addition, the gaugino mass parameters, M_2 and M_1 , are usually assumed to be related via the GUT relation

$$M_1 = \frac{5 \sin^2 \theta_W}{3 \cos^2 \theta_W} M_2. \quad (2)$$

We set the Higgs-sfermion interaction terms A_f to zero for the first and second generation fermions: $f = u, d, c, s, e, \mu$. Moreover, the masses of the gluino and first two generation squarks are set to 1.5 TeV, large enough to evade the current ATLAS and CMS limits from SUSY searches. In Tab. 2 we list the MSSM parameters needed for the evaluation of the spectrum. We now move on to a detailed description of the MSSM benchmark scenarios to be used here, known as $m_h^{\text{mod}+}$ [47] and $h\text{MSSM}$ [48].

2.1 The $m_h^{\text{mod}+}$ scenario

The $m_h^{\text{mod}+}$ scenario is a modification of the so-called maximal mixing scenario m_h^{max} [49] which was introduced to maximize M_{h^0} value by incorporating large high order effects and also to give conservative limit on $\tan\beta$ during Higgs boson searches at LEP. This scenario predicts a CP-even Higgs M_{h^0} slightly larger than the observed Higgs mass and that is why m_h^{max} scenario has been modified in order to accommodate the observed Higgs of 125 GeV. The modification is performed by reducing the amount of scalar top mixing

MSSM Scenarios	h MSSM	$m_h^{\text{mod}+}$
$\tan \beta$	1–15	1–25
M_{A^0} (GeV)	150–1000	90–1000
$M_{Q_{1,2}} = M_{U_{1,2}} = M_{D_{1,2}}$ (TeV)	-	1.5
$M_{Q_3} = M_{U_3} = M_{D_3}$ (TeV)	-	1
$M_{L_{1,2}} = M_{E_{1,2}}$ (TeV)	-	0.5
$M_{L_3} = M_{E_3}$ (TeV)	-	1
μ (TeV)	-	0.2
X_t (TeV)	-	1.5
A_t (TeV)	-	$X_t + \mu / \tan \beta$
A_b (TeV)	-	A_t
A_τ (TeV)	-	A_t
M_1 (TeV)	-	GUT relation
M_2 (TeV)	-	0.2
M_3 (TeV)	-	1.5

Table 2: MSSM input parameters for our two MSSM benchmark scenarios.

such that the mass of the lightest Higgs state, M_{h^0} , is compatible with the mass of the observed Higgs boson within ± 3 GeV as a theoretical uncertainty. When confronting $m_h^{\text{mod}+}$ with the LHC data [47], there is a substantial region in $(M_{A^0}, \tan \beta)$ plan with $\tan \beta > 7$ for which the light CP-even Higgs is in a good agreement with the measured Higgs mass at the LHC. The SUSY inputs for this scenario are given in the second column of Tab. 2 and the spectrum is computed by the use of FeynHiggs code.

2.2 The h MSSM scenario

In $m_h^{\text{mod}+}$, one needs to input M_{A^0} , $\tan \beta$ and other SUSY parameters in order to make a prediction for M_{h^0} within the allowed range, [122, 128] GeV. However, plenty of points on the $(M_{A^0}, \tan \beta)$ plane would correspond to one value of M_{h^0} , the SM-like Higgs boson mass. In order to avoid such a situation, the h MSSM was introduced [48] in which M_{h^0} was enforced to be approximately 125 GeV as well as the SUSY breaking scale $M_{\text{SUSY}} \approx M_S$ fixed to be rather high, $\gg 1$ TeV, in order to explain the non-observation of any SUSY particle at colliders. A key assumption of the h MSSM is to assume that radiative corrections to the diagonal mass of the heavy CP-even Higgs, ΔM_{22} , are much larger than the ones to the light CP-even Higgs, ΔM_{11} , and the mixing term between h and H , ΔM_{12} [48], that is: $\Delta M_{22} \gg \Delta M_{11}, \Delta M_{12}$. Therefore, ΔM_{22} , which parameterises the SUSY effects, is traded for the experimental value of M_{h^0} , $\tan \beta$ and M_Z . Therefore, the h MSSM setup describes the MSSM Higgs sector in terms of just M_{A^0} and $\tan \beta$, exactly like the tree-level predictions, given the experimental knowledge of M_Z and M_{h^0} . The SUSY input parameters in this scenario are given in the first column of Tab. 2 and the spectrum is computed by the HDECAY code [50].

3 Higgs boson masses and Branching Ratios (BR)

In our analysis, we include the measured signal rates from the ATLAS and CMS Run 2 results via Higgs-Signals-2.2.0beta [38] which returns a χ^2 value for the consistency between the model predicted signal rates and the corresponding measurements. We then determine the minimal χ^2 value over the scanned parameter space, χ_{min}^2 , and keep as allowed the portion of it that features a χ^2 value within $\Delta\chi^2 \equiv \chi^2 - \chi_{\text{min}}^2$. For every benchmark scenario, we show the $\Delta\chi^2$ behavior, the best fit point, the charged Higgs total width, the typical BRs for charged Higgs decays into various final states and the charged Higgs production cross section.

3.1 The h MSSM case

In Fig. 1, we present $\Delta\chi^2$ (top-left) and the charged Higgs total width (top-right) in the $(M_{A^0}, \tan\beta)$ plane. The best fit point is located at $M_{A^0} \approx 1$ TeV and $\tan\beta \approx 2$. The green lines show the exclusion limits from HiggsSignals at 1σ (solid) and 2σ (dashed) while the gray area is ruled out by the various LHC searches implemented in HiggsBounds. As one can see, the charged Higgs in the h MSSM scenario is rather heavy ≥ 550 GeV and the total width is large for small $\tan\beta$ and gets reduced for high $\tan\beta$ values. In the bottom panel we show the ratio Γ_{H^\pm}/M_{H^\pm} as a function of the charged Higgs mass (left) as well as a function of the charged Higgs production cross section (right). The latter can be slightly above 1 pb. It is also visible from the lower panel that the charged Higgs total width can be about 4% of the charged Higgs mass at low $\tan\beta$.

In the h MSSM scenario, the charged Higgs decays mainly into top-bottom with more than 90% BR for $\tan\beta \leq 8$, see Fig. 2 (left), which decreases for larger $\tan\beta$ values. For small $\tan\beta$, the $\text{BR}(H^+ \rightarrow t\bar{b})$ is very close to 100%. In this scenario, the $\tau\nu$ channel has a rather small BR, less than 10%, in most of the cases as depicted in Fig. 2 (right) and becomes negligible for low $\tan\beta$.

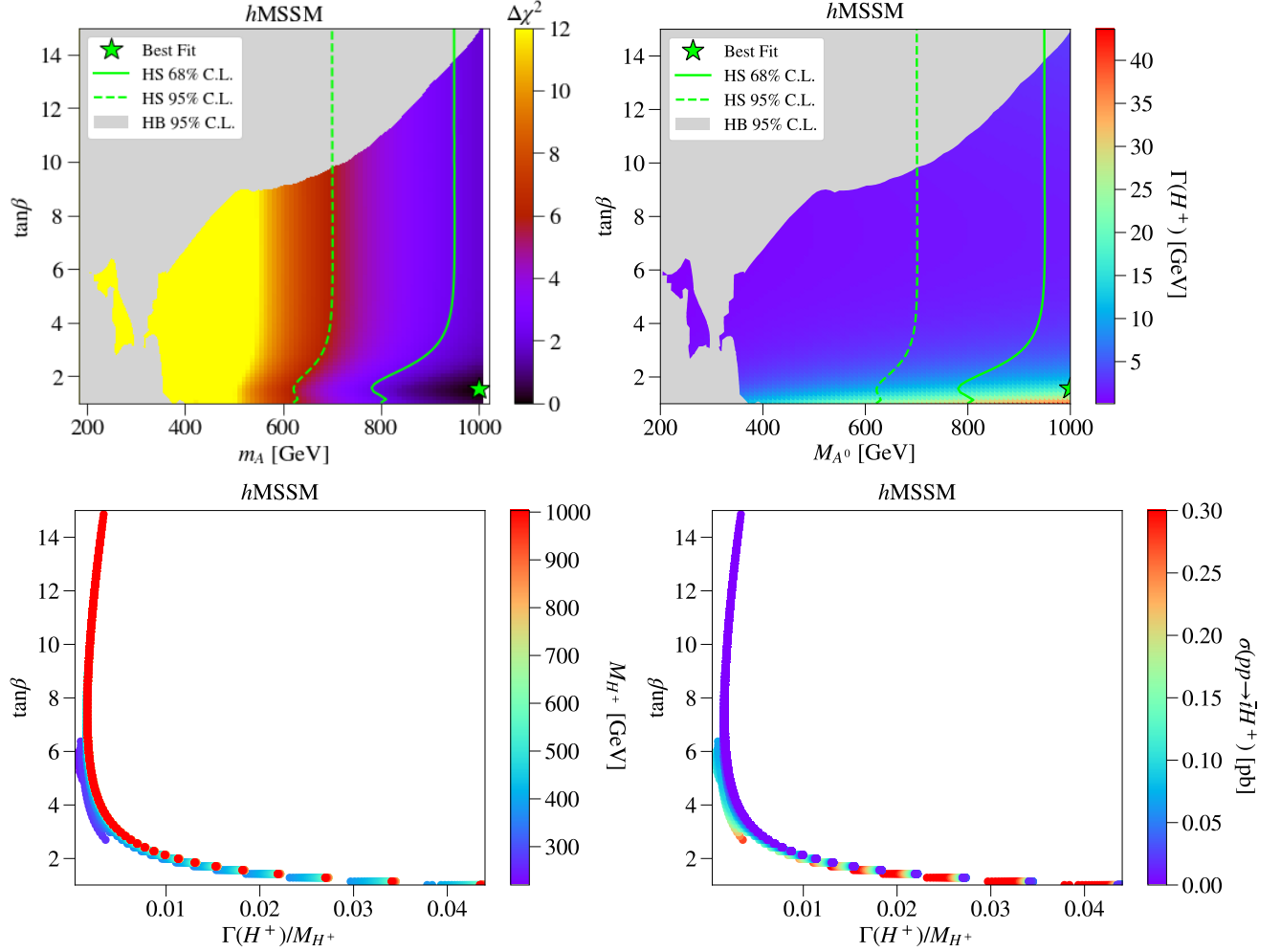


Figure 1: $\Delta\chi^2$ (top-left) and the charged Higgs total width (top-right) in the $(m_A \equiv M_{A^0}, \tan\beta)$ plane. The best fit point is located at $M_{A^0} \approx 1$ TeV and $\tan\beta \approx 2$. The green lines show the exclusion limits from HiggsSignals at 1σ (solid) and 2σ (dashed) while the gray area is ruled out by the various LHC searches implemented in HiggsBounds. The ratio Γ_{H^\pm}/M_{H^\pm} as a function of the charged Higgs mass is shown in the bottom-left panel while in the bottom-right one it is presented as a function of the charged Higgs production cross section.

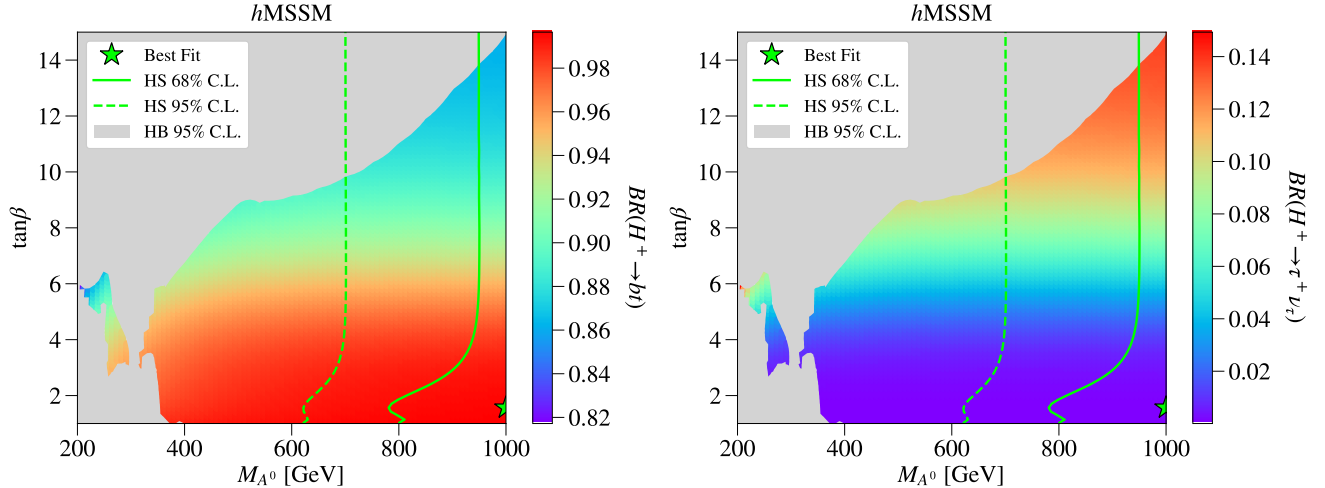


Figure 2: Allowed regions from Fig. 1 in the $(M_{A^0}, \tan\beta)$ plane for h MSSM scenario, with the color representing the BRs $\text{BR}(H^+ \rightarrow tb)$ (left) and $\text{BR}(H^+ \rightarrow \tau\nu)$ (right).

3.2 The $m_h^{\text{mod}+}$ case

In the $m_h^{\text{mod}+}$ scenario, the allowed parameter region is shown in Fig. 3 (top-left). The best fit point is located at $M_{H^\pm} \approx 1$ TeV and $\tan\beta = 20$. In order to have a low $\Delta\chi^2$ and simultaneously a light CP-even Higgs, close to 125 GeV, a value of $\tan\beta > 10$ is required. The latter requirement leads to a suppression of the total width of the charged Higgs because the BR to top-bottom is proportional to $m_t/\tan\beta$. The same argument holds for the charged Higgs production cross section which becomes smaller than in the previous scenario. The total charged Higgs width is shown in the allowed parameter region in the top-right panel of Fig. 3. Again, we need a heavy charged Higgs boson to obtain sizeable total widths but, contrary to the previous scenario, we now need quite large values of $\tan\beta$. In the two bottom panels of Fig. 3, we present $\tan\beta$ as a function of Γ_{H^\pm}/M_{H^\pm} with the colour showing the charged Higgs mass (left) and the charged Higgs production cross section (right). Clearly, a compromise has to be reached between the values chosen for the charged Higgs mass while having non-negligible values for the production cross section.

In Fig. 4, we again show the allowed region and the colour illustrates the charged Higgs BRs. In the top panels, we show $\text{BR}(H^+ \rightarrow t\bar{b})$ and $\text{BR}(H^+ \rightarrow \bar{\tau}\nu)$ where it can be seen that the tb BR is larger than the $\tau\nu$ one. In the bottom panels, we only illustrate the dominant chargino-neutralino channels, namely: $\text{BR}(H^+ \rightarrow \chi_1^0\chi_1^+)$ and $\text{BR}(H^+ \rightarrow \chi_2^0\chi_2^+)$.

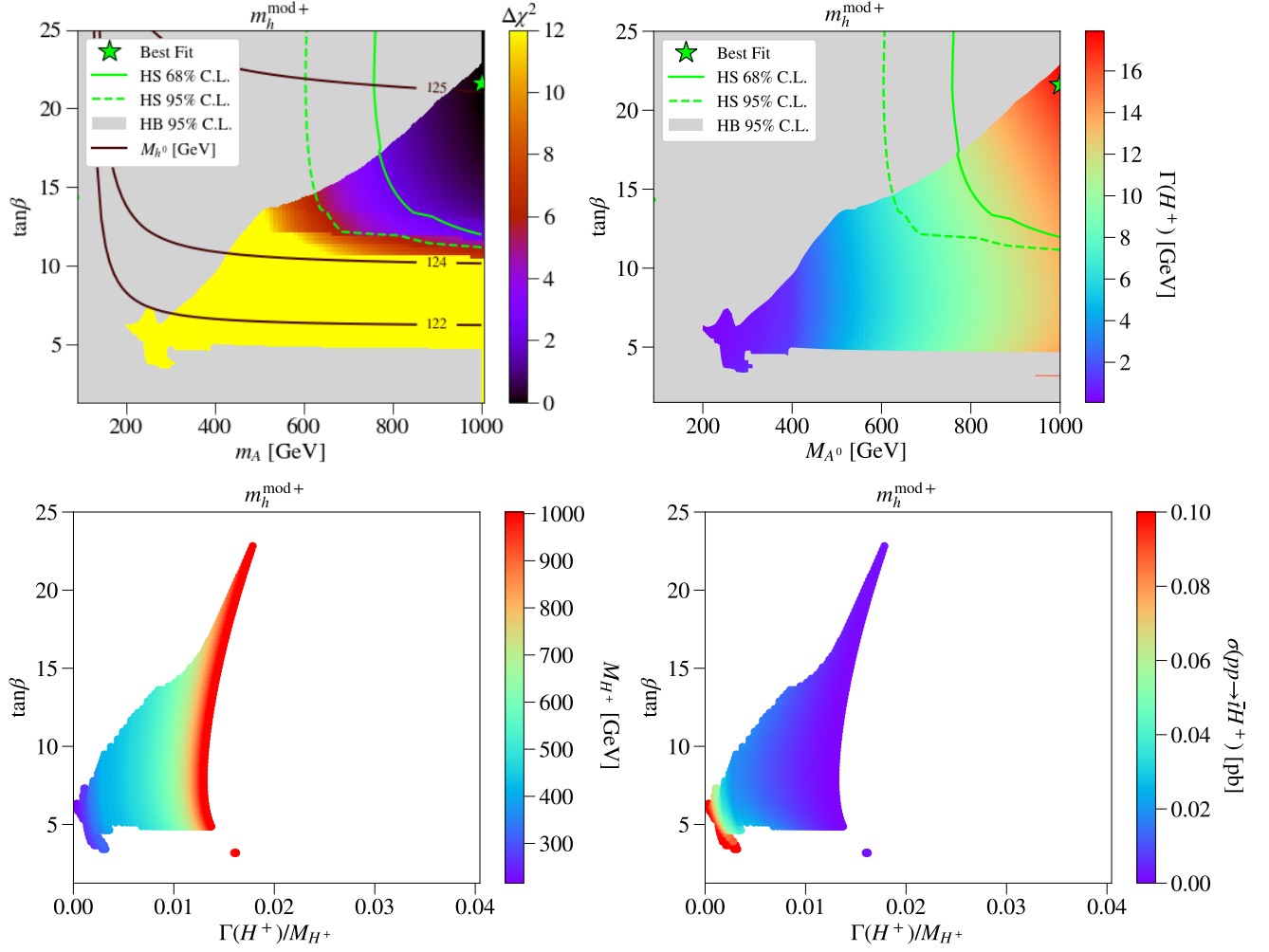


Figure 3: Allowed parameter region in the $m_h^{\text{mod}+}$ scenario over the $(m_A \equiv M_{A^0}, \tan\beta)$ plane with colour showing $\Delta\chi^2$ (top-left) and the charged Higgs boson mass (top-right). The LHC Higgs searches constraints are included. The light green contours are HiggsSignals exclusion limits at 1σ (solid) and 2σ (dashed). The light gray area is excluded by HiggsBounds at 2σ . The solid brown lines are contours for the lighter CP-even scalar h^0 mass. The best fit point is located at $M_{H^\pm} \approx 1$ TeV and $\tan\beta = 20$. In the two bottom panels of Fig. 3 we present $\tan\beta$ as a function of Γ_{H^\pm}/M_{H^\pm} with the colour code showing the charged Higgs mass (left) and the charged Higgs production cross section (right).

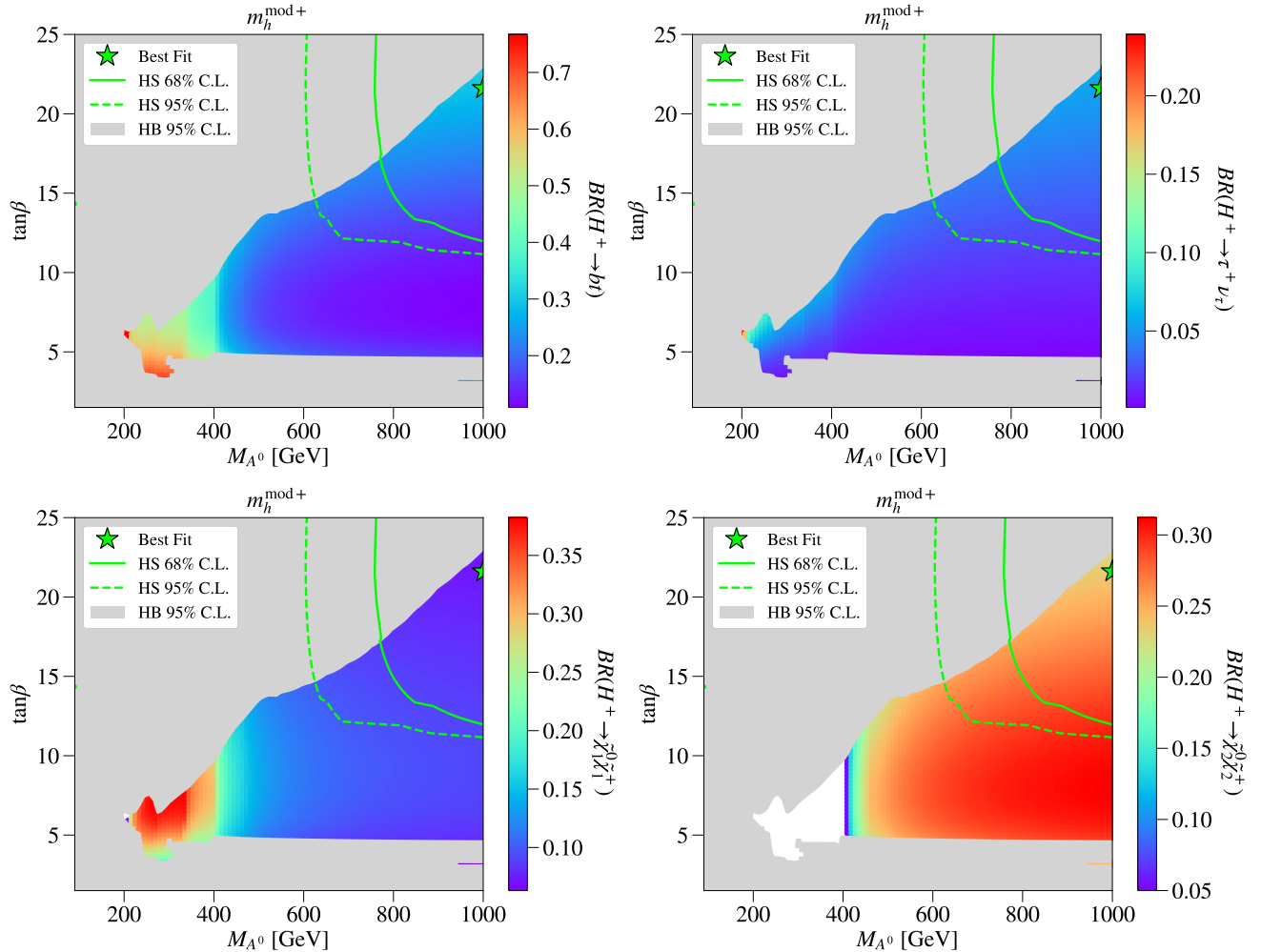


Figure 4: Allowed regions, as shown in Fig. 3, in the $(M_{A^0}, \tan\beta)$ plane. We present the BR $H^+ \rightarrow t\bar{b}$ (top-left), $H^+ \rightarrow \tau\nu$ (top-right), $H^+ \rightarrow \chi_1^0\chi_1^+$ (bottom-left) and $H^+ \rightarrow \chi_2^0\chi_2^+$ (bottom-right).

3.3 Benchmark Points (BPs)

This section briefly outlines the BPs found via the methodology outlined in the previous section.

In Tab. 3 we present four BPs for the h MSSM scenario with a value of $\tan\beta = 1.01$ and 5 and with a range of charged Higgs masses between 275 and 633.91 GeV. BP4 in this table was chosen for the numerical analysis in the following section as it has a high charged Higgs width-to-mass ratio and thus is expected to have a high interference entering the signal cross section.

In Tab. 4 we present four BPs for the $m_h^{\text{mod}+}$ scenario for a number of values of $\tan\beta$ between 3.42 and 20 and charged Higgs masses between 303.08 and 900 GeV. BP4 was chosen for the numerical analysis of the next section because it has a high cross section even though the charged Higgs width-to-mass ratio is very low. This BP provides insight into the behaviour of interference throughout the cutflow in the scenario where interference is small relative to the signal.

In both scenarios, BPs 1 to 3 are presented to motivate further research of interference in the future as they should provide interesting and, as yet un-excluded, points of the MSSM.

Parameters	BP1	BP2	BP3	BP4
MSSM inputs				
$\tan \beta$	5	5	1.01	1.01
Masses in GeV				
M_{h^0}	125	125	125	125
M_{H^0}	266.77	495.19	615.32	648.3
M_{A^0}	263	493.5	594.6	628.79
M_{H^\pm}	275.01	500	600.01	633.91
Total decay width in GeV				
$\Gamma(H^\pm)$	0.3499	1.0423	26.177	27.777
BR($H^\pm \rightarrow XY$) in %				
BR($H^\pm \rightarrow bt$)	91.665	96.105	99.375	99.418
Ratios				
$\Gamma(H^\pm)/M_{H^\pm}$	0.0012723	0.0020846	0.043628	0.043819
Cross sections in pb				
$\sigma(pp \rightarrow \bar{t}H^\pm)$	0.0932	0.0177	0.2090	0.1431
$\sigma(pp \rightarrow \bar{t}H^\pm) \times BR(H^\pm \rightarrow bt)$	0.0854	0.0170	0.2077	0.1423

Table 3: BPs for the h MSSM scenario.

4 Results

As intimated, the process studied at MC level is $pp \rightarrow t\bar{b}H^- \rightarrow t\bar{b}\bar{b}$ (+ c.c.), thus the signal is defined as all processes in the MSSM mediated by the charged Higgs with a $t\bar{b}\bar{b}$ final state while the background is defined as all processes in the MSSM with the same final state which are not mediated by a charged Higgs state. Figs. 5 and 6 present some examples of signal and background diagrams.

Let us then define the scattering interference as $I = T - S - B$ where ‘T = Total’ is the full scattering amplitude including all signal and background Feynman diagrams and the interference of these diagrams. ‘S’ is the signal scattering amplitude including only the signal diagrams and ‘B’ is the background scattering amplitude including only the background diagrams. As the same phase space is shared by all of these terms, we can perform the calculation of these terms independently and evaluate the interference via the equation presented above.

In order to explore the effects of interference on the search for a charged Higgs, we utilise BP4 found in Tab. 3 for the h MSSM case and BP4 found in Tab. 4 for the $m_h^{\text{mod}+}$ case. These two points provide two kinematically distinct scenarios, one of which - the h MSSM one - has a high width-to-mass ratio for the charged Higgs boson, of 4.4%, while the other has a much lower ratio, of 0.31%.

Signal cross sections are significantly smaller than background cross sections before cuts. Hence the simulation of the T and B terms outlined above must have low uncertainty, which requires very large MC samples. This mandates a prudent use of computing resources and thus an extremely large sample of events was generated for T, B and S at parton level to obtain a value for the cross section of these processes with very low MC error. After this was done, smaller detector level samples were generated for the purpose of applying cuts and obtaining efficiencies. The parton level cross sections and the detector level efficiencies are then used together to form the cutflow that will be presented in this section. The parton level results for both BPs can be found in Tab. 5. The error presented here is the MC error and is displayed to show that a large enough parton level sample was generated to produce a sufficiently low uncertainty on the interference cross section. There are of course other sources of errors against which to tension the size of our interference effects, such as systematic theoretical errors due to the finite order perturbative modelling of the signal and background cross sections, which can be large, especially for the latter (e.g., Ref. [21] finds that for the $t\bar{b}\bar{b}$

Parameters	BP1	BP2	BP3	BP4
MSSM inputs				
$\tan\beta$	6	10	20	3.42
Masses in GeV				
M_{h^0}	120.18	122.46	123.47	113.55
M_{H^0}	595.33	695.4	896.01	298.69
M_{A^0}	594.38	695.12	895.96	292.22
M_{H^\pm}	600	700	900	303.08
$M_{\tilde{\chi}_1^+}$	139.97	144.16	147.54	133.2
$M_{\tilde{\chi}_2^+}$	270.8	268.59	266.75	274.19
$M_{\tilde{\chi}_1^0}$	84.345	86.404	87.934	80.637
$M_{\tilde{\chi}_2^0}$	147.2	149.46	151.39	143.88
$M_{\tilde{\chi}_3^0}$	209.7	209.8	210.14	205.33
$M_{\tilde{\chi}_4^0}$	271.76	268.81	266.41	276.42
$M_{\tilde{t}_1}$	1000	999.82	996.08	998.97
$M_{\tilde{t}_2}$	1002	1002.2	1006	1002.8
$M_{\tilde{b}_1}$	876.49	876.45	876.43	876.61
$M_{\tilde{b}_2}$	1134.8	1134.8	1134.8	1134.9
Total decay width in GeV				
$\Gamma(H^\pm)$	5.8582	7.7229	14.311	0.9253
BR($H^\pm \rightarrow XY$) in %				
BR($H^\pm \rightarrow \tilde{\chi}_1^0 \tilde{\chi}_1^\pm$)	10.789	10.379	7.7896	20.73
BR($H^\pm \rightarrow \tilde{\chi}_2^0 \tilde{\chi}_2^\pm$)	27.858	29.296	24.307	—
BR($H^\pm \rightarrow \tilde{\chi}_1^\pm \tilde{\chi}_3^0$)	13.003	12.161	9.1983	—
BR($H^\pm \rightarrow \tilde{\chi}_1^\pm \tilde{\chi}_4^0$)	18.454	18.648	15.061	—
BR($H^\pm \rightarrow \tilde{\chi}_3^0 \tilde{\chi}_2^\pm$)	9.7934	11.002	9.5996	—
BR($H^\pm \rightarrow \tau^+ \nu_\tau$)	0.73738	1.8127	5.031	0.7682
BR($H^\pm \rightarrow bt$)	15.728	13.718	26.989	72.036
Ratios				
$\Gamma(H^\pm)/M_{H^\pm}$	0.0097637	0.011033	0.015901	0.0031
Cross sections in pb				
$\sigma(pp \rightarrow tH^\pm)$	0.007120	0.003170	0.002850	0.130750
$\sigma(pp \rightarrow \bar{t}H^\pm) \times BR(H^\pm \rightarrow \tilde{\chi}_1^0 \tilde{\chi}_1^\pm)$	0.000768	0.000329	0.000222	0.027100
$\sigma(pp \rightarrow \bar{t}H^\pm) \times BR(H^\pm \rightarrow \tilde{\chi}_2^0 \tilde{\chi}_2^\pm)$	0.001984	0.000929	0.000693	—
$\sigma(pp \rightarrow \bar{t}H^\pm) \times BR(H^\pm \rightarrow \tilde{\chi}_1^\pm \tilde{\chi}_3^0)$	0.000926	0.000386	0.000262	—
$\sigma(pp \rightarrow \bar{t}H^\pm) \times BR(H^\pm \rightarrow \tilde{\chi}_1^\pm \tilde{\chi}_4^0)$	0.001314	0.000591	0.000429	—
$\sigma(pp \rightarrow \bar{t}H^\pm) \times BR(H^\pm \rightarrow \tilde{\chi}_3^0 \tilde{\chi}_2^\pm)$	0.000697	0.000349	0.000274	—
$\sigma(pp \rightarrow \bar{t}H^\pm) \times BR(H^\pm \rightarrow \tau^+ \nu_\tau)$	0.000053	0.000057	0.000143	—
$\sigma(pp \rightarrow \bar{t}H^\pm) \times BR(H^\pm \rightarrow bt)$	0.001120	0.000435	0.000769	0.094200

Table 4: BPs for $m_h^{\text{mod}+}$ scenario.

background such an error is of order 10%). Further, one ought to consider the systematic errors coming with the choice of Parton Distribution Functions (PDFs) and of their factorisation/renormalisation scale, which are expected to be similar in size. Hence, one will truly need to worry about the systematic error due to the presence of the interference effects studied here when they are beyond the 10% or so level.

The parton level sample for both scenarios contained 20,000,000 events generated in MadGraph5 [51] at leading order with a Centre-of-Mass (CoM) energy of 13 TeV, while the detector level samples for the hMSSM sample contained 5,000,000 events comprised of 100 independent samples of 50,000 events and the $m_h^{\text{mod}+}$ sample contained 10,000,000 events comprised of 200 independent samples of 50,000 events. Both were generated in MadGraph5 at leading order and at 13 TeV CoM energy. The detector level samples were then sent to Pythia8 [52] for hadronisation/fragmentation and finally passed to Delphes [53] for detector smearing utilising the standard ATLAS card. Previous sections of this work calculated cross sections at

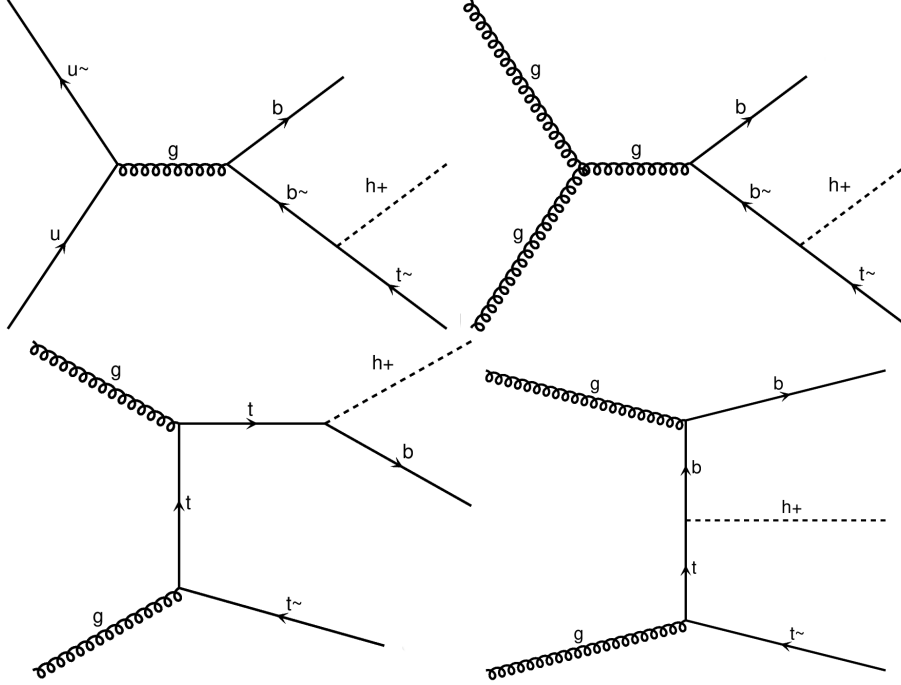


Figure 5: A selection of signal Feynman diagrams.

Model		S (pb)	B (pb)	T (pb)	I (pb)
h MSSM	σ	0.03240	13.078	13.139	0.028
	$\Delta\sigma$	1.4×10^{-5}	0.002	0.001	0.003
$m_h^{\text{mod}+}$	σ	0.08854	13.095	13.197	0.014
	$\Delta\sigma$	3.3×10^{-5}	0.001	0.001	0.002

Table 5: Parton level results for the h MSSM and $m_h^{\text{mod}+}$ benchmarks.

NLO, however, as previously explained, this is not feasible for the background samples, so the MC analysis was undertaken at LO only. All samples included the decay of the charged Higgs, $H^+ \rightarrow t\bar{b}$, to maximize statistics.

Typical detector acceptances were utilised, namely electrons and muons must have transverse momentum $p_T > 7$ GeV and pseudo-rapidity $|\eta| < 2.5$ with 100% lepton selection efficiency assumed. Jets must have $p_T > 20$ GeV and $|\eta| < 2.5$. Anti- k_T jet clustering [54] was used and a b -tagging efficiency of 77% and mistagging efficiency of 1% employed. We demand exactly one lepton in the final state, so that the longitudinal momentum of the missing energy can be solved for via

$$p_\nu^z = \frac{1}{2p_{\ell T}^2} \left(A_W p_{\ell}^z \pm E_\ell \sqrt{A_W^2 \pm 4p_{\ell T}^2 E_{\nu T}^2} \right), \quad (3)$$

where, $A_W = M_{W^\pm}^2 + 2p_{\ell T} \cdot E_{\nu T}$.

Reconstruction was then undertaken via the simultaneous minimisation of the following equations by permuting through all combinations of jets in the process,

$$\chi_{\text{had}}^2 = \frac{(M_{\ell\nu} - M_W)^2}{\Gamma_W^2} + \frac{(M_{jj} - M_W)^2}{\Gamma_W^2} + \frac{(M_{\ell\nu j} - M_T)^2}{\Gamma_T^2} + \frac{(M_{jjj} - M_T)^2}{\Gamma_T^2} + \frac{(M_{jjjj} - M_{H^\pm})^2}{\Gamma_{H^\pm}^2} \quad (4)$$

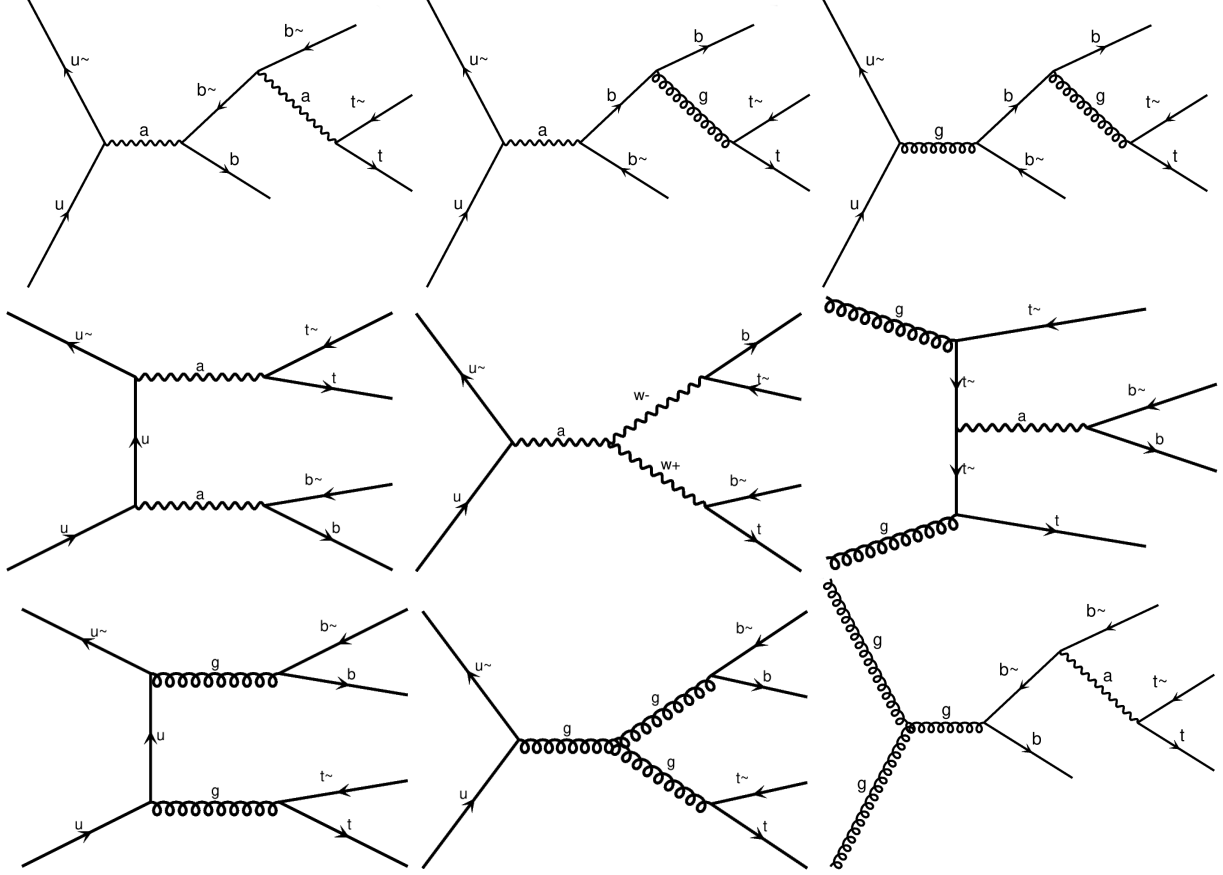


Figure 6: A selection of background Feynman diagrams.

and

$$\chi_{\text{lep}}^2 = \frac{(M_{\ell\nu} - M_W)^2}{\Gamma_W^2} + \frac{(M_{jj} - M_W)^2}{\Gamma_W^2} + \frac{(M_{\ell\nu j} - M_T)^2}{\Gamma_T^2} + \frac{(M_{jjj} - M_T)^2}{\Gamma_T^2} + \frac{(M_{\ell\nu jj} - M_{H^\pm})^2}{\Gamma_{H^\pm}^2} \quad (5)$$

The results of this reconstruction can be found in Figs. 7 and 9, normalised to unit area. This reconstruction requires one to use the width of the particles, which introduces a model dependence. Thus, in the aforementioned figures, we also present the same reconstruction methodology but without the use of particle widths to highlight how this affects the reconstruction. We refer to these methodologies as the model dependent and model independent reconstructions, respectively.

We apply a simple set of acceptance cuts to illustrate the sensitivity to the interference term, these cuts include a final state definition of 1 lepton, 5 or more jets, more than 2 or 3 b -jets, greater than 20 GeV missing transverse energy and, finally, the transverse mass of missing energy and the lepton must be higher than 60 GeV. Specifically, $m_T^W = \sqrt{(\cancel{E}_x + \ell_x)^2 + (\cancel{E}_y + \ell_y)^2} > 60$ GeV. It is an interesting question to experimentalists as to how interference contributions change with respect to varying b -tagging. This motivates the usage of 2 and 3 b -tags regions even if the increased b -tagging does not necessarily lead to increased signal significance. This cutflow, applied to each of the BPs, can be found in Tabs. 6 and 7.

4.1 The h MSSM analysis

It can be seen in Fig. 7 that all particles appear to be reconstructed very well. The model-dependent reconstruction and the model-independent case perform equally well for the signal. However, for the background and total samples the reconstruction is quite different. The model-dependent assumption provides a much better separation from the signal, this is especially apparent in both the leptonic and hadronic charged Higgs invariant mass distributions.

The ratio of signal cross section to interference cross section before cuts is 86.7%. This is an alarmingly high level of interference that a traditional experimental study would not account for correctly. The ratio after cuts in both the ≥ 2 b -tag scenario and ≥ 3 b -tag scenarios is 103.3% and 85.5% respectively, both extremely large interferences showing that the cutflow has done little to mitigate the magnitude of the interference relative to the signal. It should be noted that the uncertainty on the values in the ≥ 3 b -tag region are approaching the same magnitude as the interference itself, thus strong conclusions in this region cannot be made.

It is important to note that the true effect of the interference is predicated on the overall shape of the interference distribution relative to the signal distribution. In general there are three cases [55–57]:

1. The interference takes the same shape as the signal and is positive, here we can expect a boosting of our new physics effects.
2. The interference takes the same shape as the signal and is negative, here we expect a cancellation of our new physics effects.
3. The interference takes a different shape and is either positive or negative, here we can expect a boosting and cancellation of new physics effects in different regions of phase space, manifesting as a “peak-dip” structure in the expected distributions.

In Fig. 8, an exploration of this shape at parton level before cuts can be seen in the $t\bar{t}b\bar{b}$ reconstructed invariant mass plane. This step was undertaken at parton level to achieve the required per-bin statistics to discern the shape of the interference distribution. There appears to be a large interference impact in across the whole mass range, interestingly though the largest contributions are below the charged Higgs mass peak. The result of this would likely be a smearing of the charged Higgs mass bump towards lower values in actual data.

Cut	S	B	T	I	ΔI
No cuts:	9720	3923550	3941700	8429	2487
$N_\ell = 1$:	2160	904247	907925	1518	1193
$N_J \geq 5$:	1938	624001	627534	1594	992
$N_{BJ} \geq 2$:	1511	404919	408054	1623	799
$\cancel{E} > 20$ GeV:	1435	373648	376517	1433	768
$\cancel{E} + m_T^W > 60$ GeV:	1412	364026	366898	1458	758
Cut	S	B	T	I	ΔI
$N_{BJ} \geq 3$:	826	171918	173430	684	521
$\cancel{E} > 20$ GeV:	785	158921	160376	669	501
$\cancel{E} + m_T^W > 60$ GeV:	772	154880	156314	660	494

Table 6: Cut flow results presented in expected event yield with 300 fb^{-1} of luminosity for the h MSSM benchmark with 5,000,000 events for each sample.

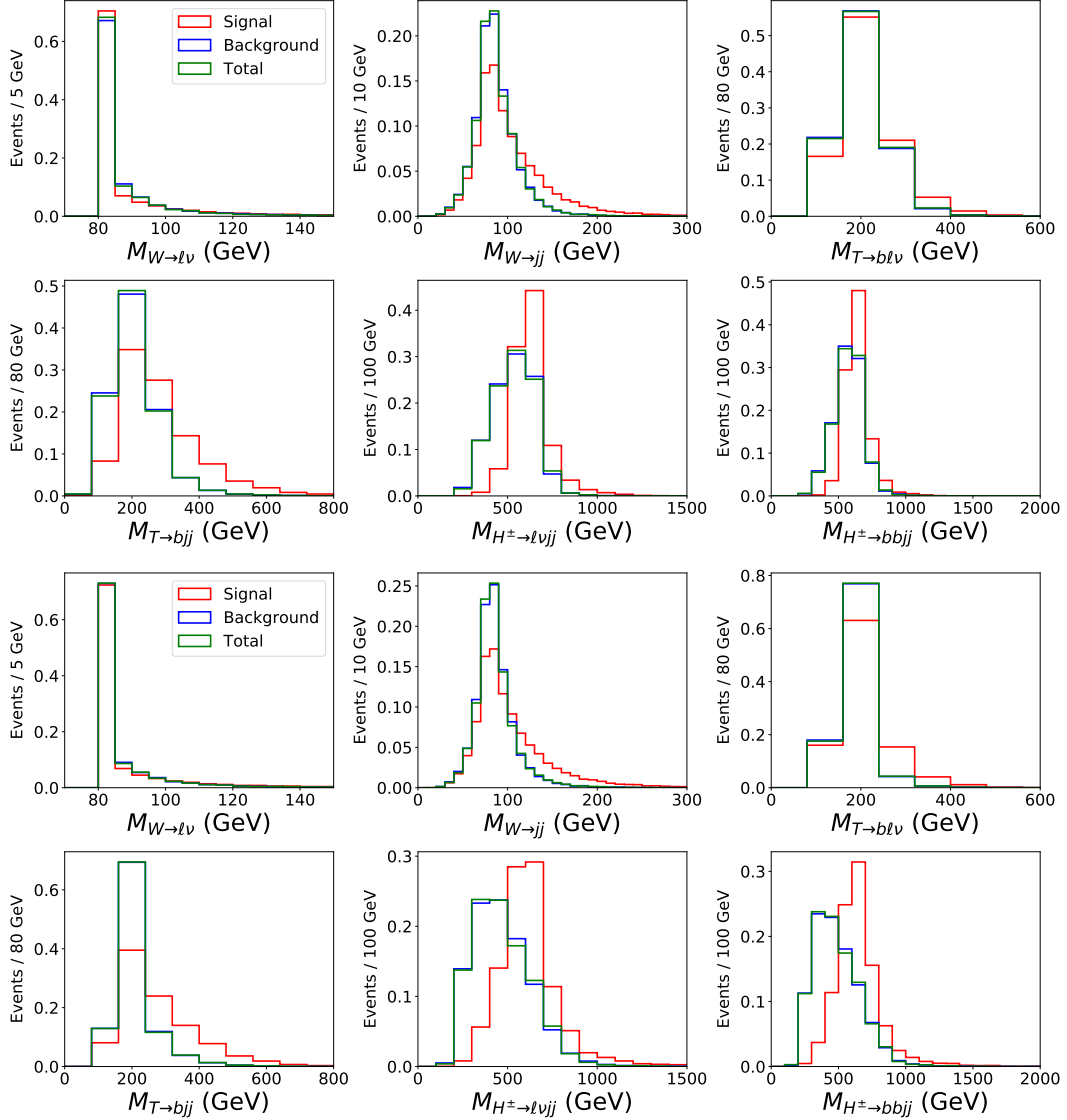


Figure 7: Invariant mass distributions for reconstructed particles in the h MSSM benchmark. Top: Model independent. Bottom: Model dependent.

4.2 The $m_h^{\text{mod}+}$ analysis

The reconstruction in this scenario presents far less distinct signal distributions, which can be seen in the charged Higgs invariant mass plots of Fig. 9. As the mass difference between the charged Higgs and the sum of the t and b -quark masses is far smaller in this scenario, it appears that the reconstruction is performed very similarly for the signal and background. This can be further seen in the lack of difference between the model-dependent and model-independent reconstructions. Thus, extraction of the signal would be far more difficult in this case.

As the ratio of the charged Higgs mass to charged Higgs width is smaller in this benchmark than in the h MSSM one, we expect the interference effects to be smaller. However, the interference may become much larger relative to the signal after a cutflow. Tab. 7 displays the cutflow results for this BP and one can see

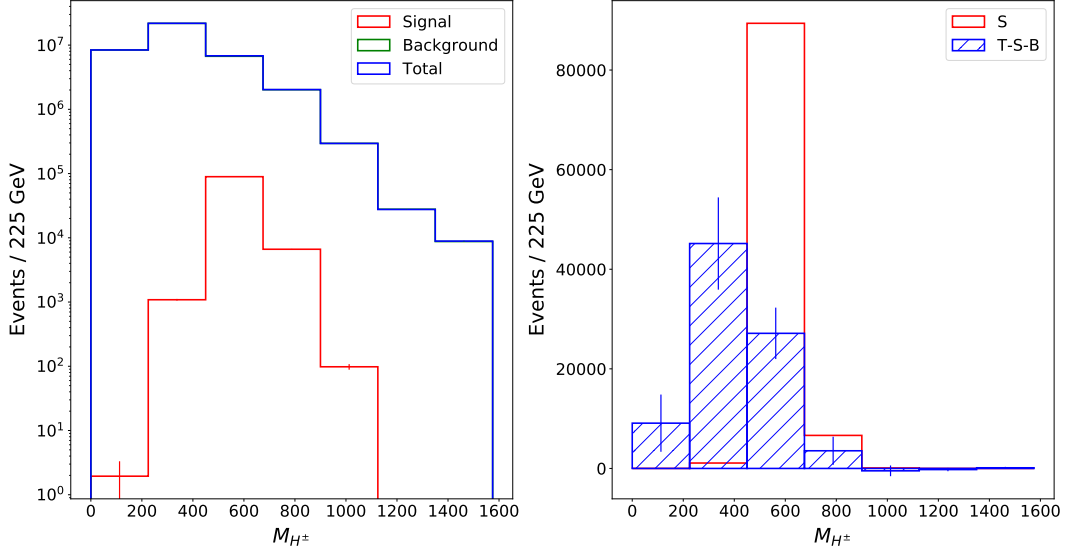


Figure 8: The charged Higgs invariant mass distribution of the signal, background and total samples (left) and interference and signal (right) at parton level and without cuts in the h MSSM scenario.

that the pre-cut ratio of interference cross section to signal cross section is 15.2%, while the ratio after cuts in the ≥ 2 b -tag region is 26.0%. In this scenario the more strict use of b -tagging decreased the ratio of the interference cross section to the signal cross section to 17.4%, though it should be noted the uncertainty on the values in the ≥ 3 b -tag region has grown beyond the magnitude of interference and conclusions in this region are tenuous.

Cut	S	B	T	I	ΔI
No cuts:	26561	3928500	3959100	4038	1764
$N_\ell = 1$:	6017	903764	911292	1510	846
$N_J \geq 5$:	4964	623989	629532	578	703
$N_{BJ} \geq 2$:	3704	404776	409342	862	566
$\cancel{E} > 20$ GeV:	3432	373464	377885	989	544
$\cancel{E} + m_T^W > 60$ GeV:	3342	363876	368087	868	537
Cut	S	B	T	I	ΔI
$N_{BJ} \geq 3$:	1894	171654	173822	273	369
$\cancel{E} > 20$ GeV:	1757	158581	160686	347	354
$\cancel{E} + m_T^W > 60$ GeV:	1712	154576	156587	298	350

Table 7: Cut flow results presented in expected event yield with 300 fb^{-1} of luminosity for the $m_h^{\text{mod}+}$ benchmark with 10,000,000 events for each sample.

The interference shape of the reconstructed invariant mass of $t\bar{t}b\bar{b}$ at parton level and before cuts in this scenario can be found in Fig 10. In this scenario the signal invariant mass distribution peaks narrowly over the 300 GeV bin, however, interestingly the interference distribution appears to be a widely spread spectrum across the range 100 – 350 GeV. These small, but non-negligible, interference contributions would likely lead to a widening of an otherwise sharp signal bump in data, which further motivates the necessity of the signal shape analysis at detector level to discover whether this effect would be dominated by the smearing effect of the detector on the signal peak.

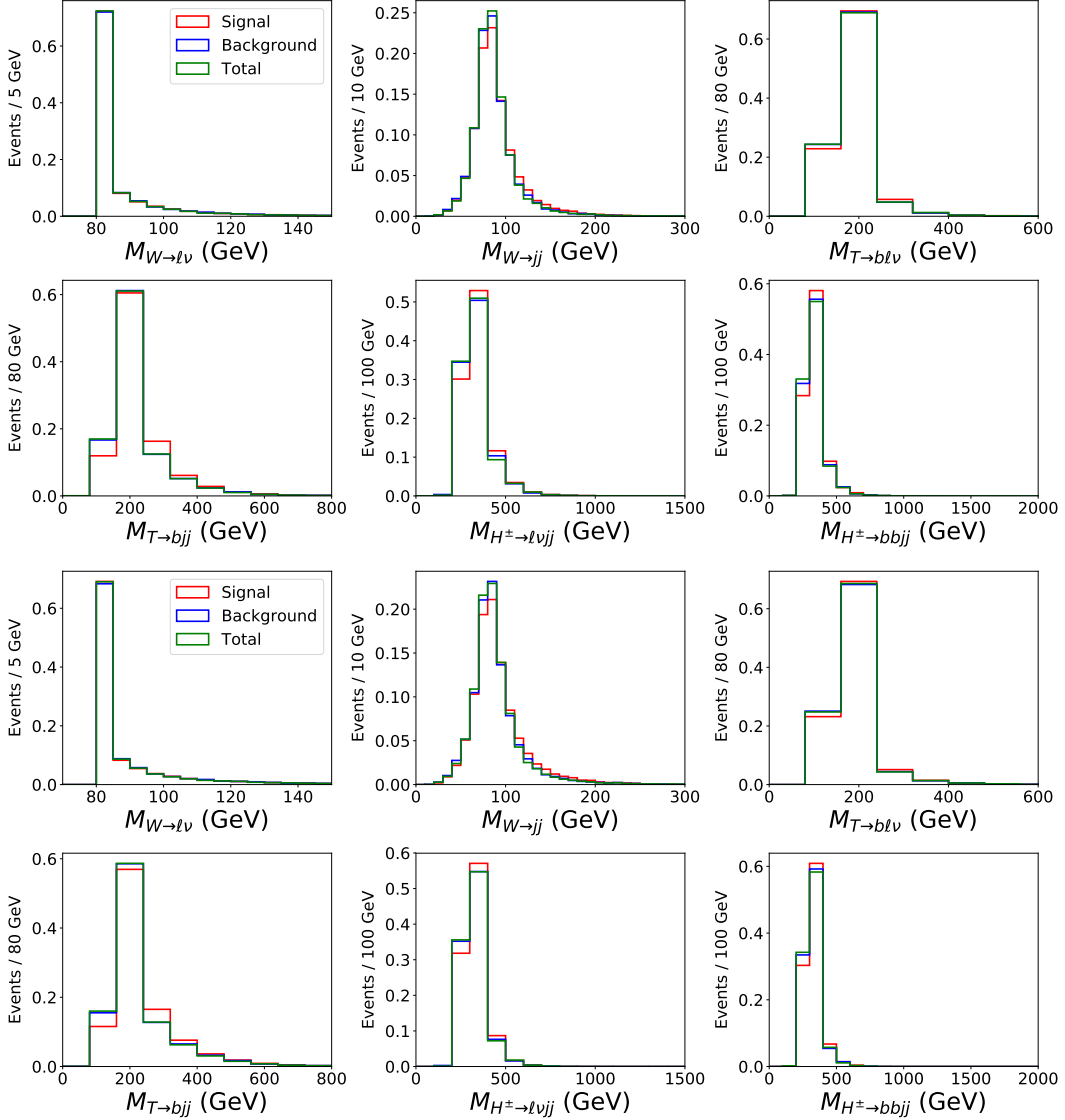


Figure 9: Invariant mass distributions for reconstructed particles in the $m_h^{\text{mod}+}$ benchmark. Top: Model independent. Bottom: Model dependent.

5 Conclusions

By borrowing the MSSM as a theoretical template that contains charged Higgs bosons, we have shown how experimental searches for these states cannot be made immune from large interference effects between signal and background whenever they have a large mass and a width on the order of one percent of the mass and upwards. We have illustrated this for the case of the $H^+ \rightarrow t\bar{b}$ decay channel, which is onset dominantly by $gg \rightarrow b\bar{t}H^+$ production. In this case, the (irreducible) background intervening in such interference effects is $pp \rightarrow t\bar{t}b\bar{b}$, which can see both QCD and EW interactions. This study's goal was to show that signal and background are wrongly treated as separate in current LHC approaches.

In order to realistically assess the above phenomenon, we have decayed the $t\bar{t}$ pair semi-leptonically and carried out a full parton shower, hadronisation and detector analysis. In doing so, we have first prepared the

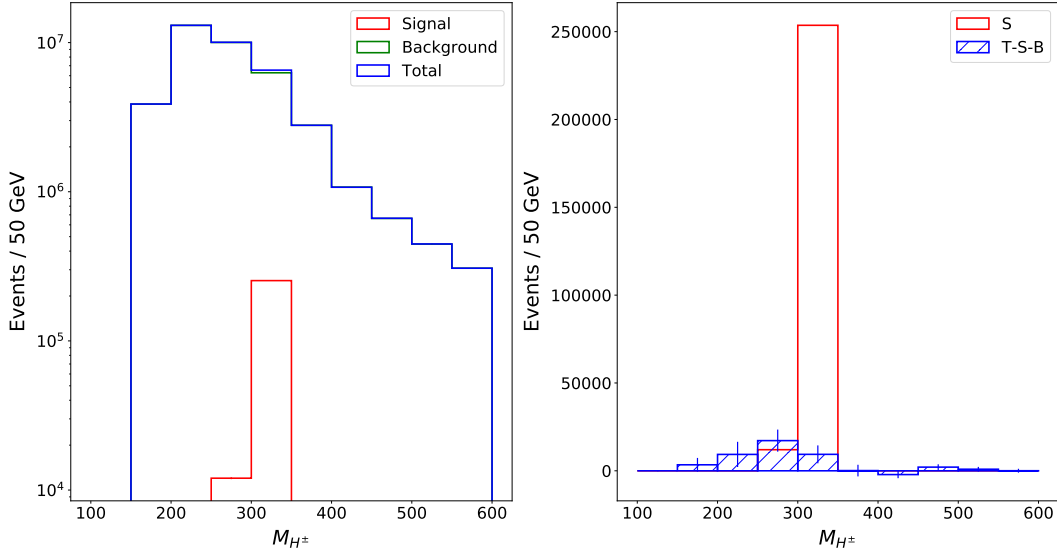


Figure 10: The charged Higgs invariant mass distribution of the signal, background and total samples (left) and interference and signal (right) at parton level and without cuts in the $m_h^{\text{mod}+}$ scenario.

MSSM parameter space regions amenable to phenomenological investigation by enforcing both theoretical (i.e., unitarity, perturbativity, vacuum stability, triviality) and experimental (i.e., from flavour physics, void and successful Higgs boson searches at the Tevatron and LHC, EW precisions observables from LEP and SLC) constraints, assuming two benchmark configurations of the MSSM, the so-called h MSSM and $m_h^{\text{mod}+}$ scenarios.

After performing a sophisticated MC simulation, allowing for both model-independent and model-dependent selections, we have seen that such interference effects can be very large, even of $\mathcal{O}(100\%)$, both before and after H^\pm detection cuts are enforced. This appears to be the case for the masses tested, approximately 300 and 630 GeV, in the MSSM scenarios adopted, though interference effects will manifest themselves at different LHC stages, depending on the overall cross sections, which vary significantly from one benchmark to another. Furthermore, the shapes of the signal and its interference (with the aforementioned irreducible background) appear to be different which would mean that it is not actually possible to proceed to a rescaling of the event yields due solely to the signal. In turn, in experimental analyses, one should account for such interference effects at the event generation level. We have proven this to be the case for a standard cut flow, while deferring the study of similar effects in the case of a machine learning framework to a future publication.

Before closing, though, we highlight the fact that the aforementioned results have been obtained in presence of a statistical error that (in some, but not all, cases) competes with the size of the interferences themselves, owing to a limitation of our computing resources. Nonetheless, in all cases we were able to obtain rather stable cutflows, wherein the increase in statistics essentially reduced the errors as expected without significantly altering the central values of our predictions. On the basis of this, we advocate future experimental analyses with larger data samples to establish the exact extent of such interference effects.

Acknowledgements

AA, DA, RB, HH, SM and RS are partially supported by the H2020-MSCA-RISE-2014 grant no. 645722 (NonMinimalHiggs). SM is further supported through the NExT Institute and the STFC Consolidated Grant ST/L000296/1. DA and RS are further supported in part by the CERN fund grant CERN/FIS-

PAR/0002/2017, by an FCT grant PTDC/FIS-PAR/31000/2017, by the CFTC-UL projects UIDB/00618/2020 and UIDP/00618/2020, and by the HARMONIA project under contract UMO-2015/18/M/ST2/00518. RP is supported by the University of Adelaide and the Australian Research Council through the ARC Center of Excellence for Particle Physics (CoEPP) at the Terascale (grant no. CE110001004). This work is also supported by the Moroccan Ministry of Higher Education and Scientific Research MESRSFC and CNRST, Project PPR/2015/6. We thank Pietro Slavich and Bill Murray for discussions.

References

- [1] G. Aad *et al.* [ATLAS Collaboration], Phys. Lett. B **716**, 1 (2012) [arXiv:1207.7214 [hep-ex]].
- [2] S. Chatrchyan *et al.* [CMS Collaboration], Phys. Lett. B **716**, 30 (2012) [arXiv:1207.7235 [hep-ex]].
- [3] G. Aad *et al.* [ATLAS and CMS Collaborations], Phys. Rev. Lett. **114**, 191803 (2015) [arXiv:1503.07589 [hep-ex]].
- [4] G. Aad *et al.* [ATLAS and CMS Collaborations], JHEP **1608**, 045 (2016) [arXiv:1606.02266 [hep-ex]].
- [5] S. Moretti and S. Khalil, “Supersymmetry Beyond Minimality: From Theory to Experiment”, CRC Press (Taylor & Francis), December 2017.
- [6] H. P. Nilles, Phys. Rept. **110**, 1 (1984).
- [7] H. E. Haber and G. L. Kane, Phys. Rept. **117**, 75 (1985)
- [8] V. D. Barger, R. J. N. Phillips and D. P. Roy, Phys. Lett. B **324**, 236 (1994) [arXiv:hep-ph/9311372];
J. F. Gunion, H. E. Haber, F. E. Paige, W. K. Tung and S. S. D. Willenbrock, Nucl. Phys. B **294**, 621 (1987);
R. M. Barnett, H. E. Haber and D. E. Soper, Nucl. Phys. B **306**, 697 (1988);
J. L. Diaz-Cruz and O. A. Sampayo, Phys. Rev. D **50**, 6820 (1994);
F. Borzumati, J. L. Kneur and N. Polonsky, Phys. Rev. D **60**, 115011 (1999) [hep-ph/9905443].
- [9] K. Assamagan, M. Guchait and S. Moretti, [arXiv:hep-ph/0402057 [hep-ph]].
- [10] M. Guchait and S. Moretti, JHEP **01**, 001 (2002) [arXiv:hep-ph/0110020 [hep-ph]].
- [11] A. G. Akeroyd *et al.*, Eur. Phys. J. C **77**, no. 5, 276 (2017) [arXiv:1607.01320 [hep-ph]].
- [12] G. Aad *et al.* [ATLAS Collaboration], JHEP **1503**, 088 (2015) [arXiv:1412.6663 [hep-ex]].
- [13] V. Khachatryan *et al.* [CMS Collaboration], JHEP **1511**, 018 (2015) [arXiv:1508.07774 [hep-ex]].
- [14] A. M. Sirunyan *et al.* [CMS Collaboration], arXiv:1903.04560 [hep-ex].
- [15] M. Aaboud *et al.* [ATLAS Collaboration], JHEP **1809**, 139 (2018) [arXiv:1807.07915 [hep-ex]].
- [16] D. J. Miller, S. Moretti, D. P. Roy and W. J. Stirling, Phys. Rev. D **61**, 055011 (2000) [hep-ph/9906230].
- [17] S. Moretti and D. Roy, Phys. Lett. B **470**, 209-214 (1999) [arXiv:hep-ph/9909435 [hep-ph]].
- [18] M. Aaboud *et al.* [ATLAS Collaboration], Phys. Lett. B **759**, 555 (2016) [arXiv:1603.09203 [hep-ex]].
- [19] CMS Collaboration [CMS Collaboration], CMS-PAS-HIG-16-031.
- [20] The ATLAS collaboration [ATLAS Collaboration], ATLAS-CONF-2016-089.
- [21] M. Aaboud *et al.* [ATLAS], JHEP **11**, 085 (2018) [arXiv:1808.03599 [hep-ex]].
- [22] F. Moortgat, S. Abdullin and D. Denegri, [arXiv:hep-ph/0112046 [hep-ph]].

- [23] M. Bisset, N. Kersting, J. Li, F. Moortgat, S. Moretti and Q. Xie, Eur. Phys. J. C **45**, 477-492 (2006) [arXiv:hep-ph/0501157 [hep-ph]].
- [24] M. Bisset, M. Guchait and S. Moretti, Eur. Phys. J. C **19**, 143-154 (2001) [arXiv:hep-ph/0010253 [hep-ph]].
- [25] M. Bisset, F. Moortgat and S. Moretti, Eur. Phys. J. C **30**, 419-434 (2003) [arXiv:hep-ph/0303093 [hep-ph]].
- [26] A. Arhrib, R. Benbrik, S. Moretti, R. Santos and P. Sharma, Phys. Rev. D **97**, no. 7, 075037 (2018) [arXiv:1712.05018 [hep-ph]].
- [27] S. Heinemeyer, W. Hollik and G. Weiglein, Eur. Phys. J. C **9**, 343 (1999) [hep-ph/9812472].
- [28] S. Heinemeyer, W. Hollik and G. Weiglein, Phys. Rev. D **58**, 091701 (1998) [hep-ph/9803277].
- [29] S. Heinemeyer, W. Hollik and G. Weiglein, Phys. Lett. B **440**, 296 (1998) [hep-ph/9807423].
- [30] G. Degrossi, S. Heinemeyer, W. Hollik, P. Slavich and G. Weiglein, Eur. Phys. J. C **28**, 133 (2003) [hep-ph/0212020].
- [31] W. Beenakker, R. Hopker and M. Spira, [arXiv:hep-ph/9611232 [hep-ph]].
- [32] S. Heinemeyer, W. Hollik and G. Weiglein, Comput. Phys. Commun. **124**, 76 (2000) [hep-ph/9812320].
- [33] T. Hahn, S. Heinemeyer, W. Hollik, H. Rzehak and G. Weiglein, Comput. Phys. Commun. **180**, 1426 (2009)
- [34] P. Bechtle, O. Brein, S. Heinemeyer, G. Weiglein and K. E. Williams, Comput. Phys. Commun. **181**, 138 (2010) [arXiv:0811.4169 [hep-ph]].
- [35] P. Bechtle, O. Brein, S. Heinemeyer, G. Weiglein and K. E. Williams, Comput. Phys. Commun. **182**, 2605 (2011) [arXiv:1102.1898 [hep-ph]].
- [36] P. Bechtle, O. Brein, S. Heinemeyer, O. Stål, T. Stefaniak, G. Weiglein and K. E. Williams, Eur. Phys. J. C **74**, no. 3, 2693 (2014) [arXiv:1311.0055 [hep-ph]].
- [37] P. Bechtle, S. Heinemeyer, O. Stål, T. Stefaniak and G. Weiglein, Eur. Phys. J. C **75**, no. 9, 421 (2015) [arXiv:1507.06706 [hep-ph]].
- [38] P. Bechtle, S. Heinemeyer, O. Stål, T. Stefaniak and G. Weiglein, Eur. Phys. J. C **74**, no. 2, 2711 (2014) [arXiv:1305.1933 [hep-ph]].
- [39] [LEP Higgs Working Group for Higgs boson searches, ALEPH, DELPHI, L3 and OPAL], [arXiv:hep-ex/0107031 [hep-ex]].
- [40] J. Abdallah *et al.* [DELPHI], Eur. Phys. J. C **34**, 399-418 (2004) [arXiv:hep-ex/0404012 [hep-ex]].
- [41] V. M. Abazov *et al.* [D0 Collaboration], Phys. Lett. B **682**, 278 (2009) [arXiv:0908.1811 [hep-ex]].
- [42] T. Aaltonen *et al.* [CDF Collaboration], Phys. Rev. Lett. **103**, 101803 (2009) [arXiv:0907.1269 [hep-ex]].
- [43] CDF collaboration, CDF Note 7712.
- [44] CDF collaboration, CDF Note 8353.
- [45] G. Aad *et al.* [ATLAS Collaboration], JHEP **1206**, 039 (2012) [arXiv:1204.2760 [hep-ex]].
- [46] A. Arhrib, R. Benbrik, H. Harouiz, S. Moretti and A. Rouchad, [arXiv:1810.09106 [hep-ph]].
- [47] M. Carena, S. Heinemeyer, O. Stål, C. E. M. Wagner and G. Weiglein, Eur. Phys. J. C **73** no.9, 2552 (2013) [arXiv:1302.7033 [hep-ph]].

- [48] A. Djouadi, L. Maiani, G. Moreau, A. Polosa, J. Quevillon and V. Riquer, Eur. Phys. J. C **73**, 2650 (2013) [arXiv:1307.5205 [hep-ph]].
- L. Maiani, A. D. Polosa and V. Riquer, New J. Phys. **14**, 073029 (2012) [arXiv:1202.5998 [hep-ph]].
- L. Maiani, A. D. Polosa and V. Riquer, Phys. Lett. B **718**, 465 (2012) [arXiv:1209.4816 [hep-ph]].
- A. Djouadi and J. Quevillon, JHEP **1310**, 028 (2013) [arXiv:1304.1787 [hep-ph]].
- A. Djouadi, L. Maiani, A. Polosa, J. Quevillon and V. Riquer, JHEP **1506**, 168 (2015) [arXiv:1502.05653 [hep-ph]].
- [49] S. Heinemeyer, W. Hollik and G. Weiglein, JHEP **06**, 009 (2000) [arXiv:hep-ph/9909540 [hep-ph]].
- [50] A. Djouadi, J. Kalinowski and M. Spira, Comput. Phys. Commun. **108**, 56-74 (1998) [arXiv:hep-ph/9704448 [hep-ph]].
- A. Djouadi, J. Kalinowski, M. Muehlleitner and M. Spira, Comput. Phys. Commun. **238**, 214 (2019) [arXiv:1801.09506 [hep-ph]].
- [51] J. Alwall *et al.*, JHEP **1407**, 079 (2014) [arXiv:1405.0301 [hep-ph]].
- [52] T. Sjöstrand *et al.*, Comput. Phys. Commun. **191**, 159 (2015) [arXiv:1410.3012 [hep-ph]].
- [53] J. de Favereau *et al.* [DELPHES 3 Collaboration], JHEP **1402**, 057 (2014) [arXiv:1307.6346 [hep-ex]].
- [54] M. Cacciari, G. P. Salam and G. Soyez, JHEP **0804**, 063 (2008) [arXiv:0802.1189 [hep-ph]].
- [55] K.J.F. Gaemers and F. Hoogeveen, Phys. Lett. B **146**, 347-349 (1984).
- [56] D. Dicus, A. Stange and S. Willenbrock, Phys. Lett. B **333**, 126 (1994).
- [57] J. Song, and Y.W. Yoon and S. Jung, Phys. Rev. D **93**, no. 5, 055035 (2016) [arXiv:1510.03450 [hep-ph]].